Electronic Supplementary Material (ESI) for Green Chemistry.

Electronic Supplementary Information

Valorisation of agricultural waste with adsorption/nanofiltration hybrid process: from materials to sustainable process design

Christos Didaskalou,[a] Sibel Buyuktiryaki,[b] Rustem Kecili,[b] Claudio P. Fonte[a] and Gyorgy Szekely[a,*]

[a]School of Chemical Engineering & Analytical Science, The University of Manchester, The Mill, Sackville Street, Manchester, M13 9PL, United Kingdom

[b]Yunus Emre Vocational School, Anadolu University, Eskisehir, 26470, Turkey

* Corresponding author: +44(0)161 306 4366, gyorgy.szekely@manchester.ac.uk,

Table of Contents

1. Synthesis of the Functional Monomers

1.1 Synthesis of 1-(4-vinylphenyl)-3-(3,5-bis(trifluoromethyl)phenyl)urea (FM3)

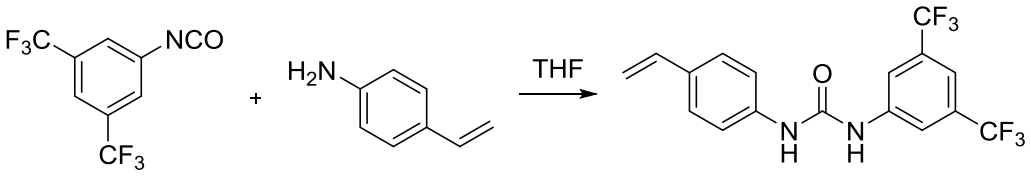

Fig. S1 Synthesis of 1-(4-vinylphenyl)-3-(3,5-bis(trifluoromethyl)phenyl)urea functional monomer using 3,5-bis(trifluoromethyl)phenyl isocyanate and 4-vinylaniline in tetrahydrofurane.

The synthesis of the urea functional monomer the previously reported method by Hall *et al.* was followed.[1] To a stirred solution of 4-vinylaniline (20 mmol) in tetrahydrofuran (50 mL) under an inert atmosphere was added 3,5-bis(trifluoromethyl)phenyl isocyanate (20 mmol). The solution was allowed to stir at room temperature overnight and then the solvent was evaporated under reduced pressure. The resulting solid residue was recrystallized from ethanol. Yield: 62%.

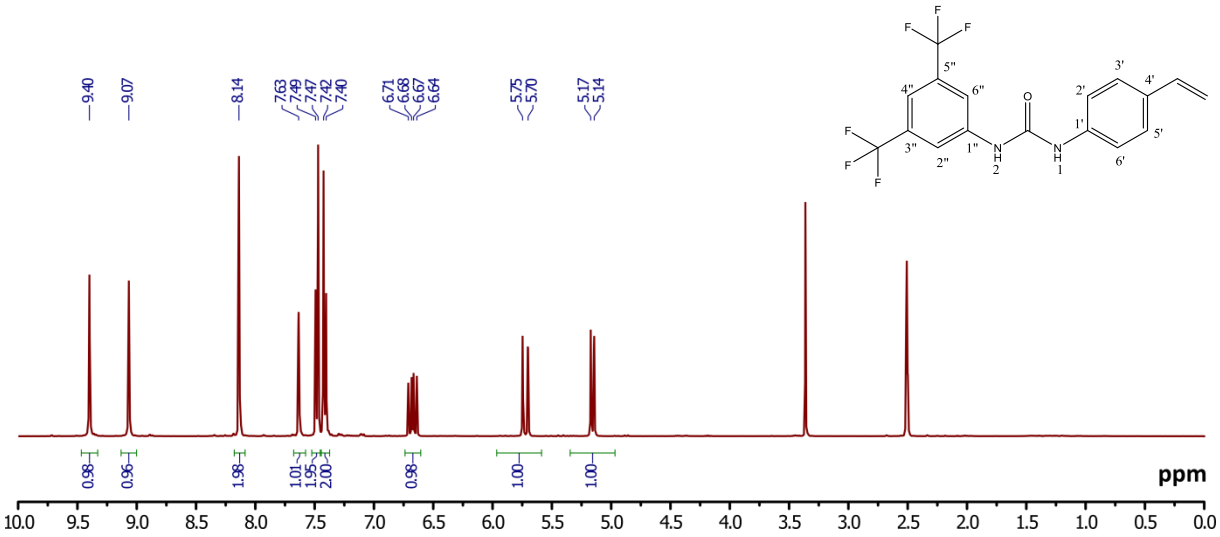

Fig. S2 ^{1}H-NMR spectrum of 1-(4-vinylphenyl)-3-(3,5-bis(trifluoromethyl)phenyl)urea functional monomer. ^{1}H-NMR (400 MHz, DMSO-d_6) δ: 5.16 (1H, dd, *J*=10.8 Hz, 0.8 Hz, CH=CH_2), 5.73 (1H, dd, *J*=17.6 Hz, 0.8 Hz, CH=CH_2), 6.68 (1H, dd, J_{AB}=10.8 Hz, C*H*=CH$_2$), 7.41 and 7.48 (2×2H, dd, $J_{AA'BB'}$=8.6 Hz, Ar-CH-2',6' and Ar-CH-3',5'), 7.63 (1H, s, Ar-CH-4"), 8.14 (2H, s, Ar-CH-2", 6"), 9.07 (1H, s, urea-NH-3), 9.40 (1H, s, urea-NH-1) ppm.

1.2 Synthesis of methacryloyl benzotriazole functional monomer for FM5

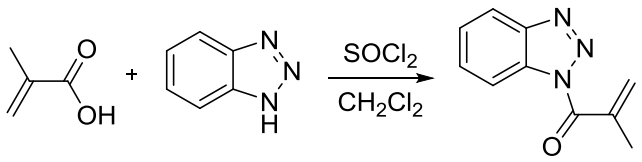

Fig. S3 Synthesis of methacryloyl benzotriazole using methacrylic acid, 1,2,3-benzotriazole and thionyl chloride in dichloromethane.

The synthesis of the methacryloyl benzotriazole functional monomer the previously reported method by Katritzky *et al*. was followed[2] To a stirred solution of benzotriazole (4.8 g, 40 mmol) in dichloromethane (50 mL) was added thionyl chloride (1.2 g, 10 mmol) at 25 °C. After 30 min, methacrylic acid (10 mmol) was added in one portion and stirring was continued for 2 h. The white precipitate was filtered off and washed with dichloromethane (3 × 60 mL). The combined organic solution was washed with aqueous 1 M NaOH (3 × 60 mL), dried over Na_2SO_4 and the solvent was removed under reduced pressure. The residue was purified by flash chromatography using silica gel and hexane:ethyl acetate (4:1) eluent. Yield: 94%. After synthesis, the monomer was stored at 5 °C and further used within a week to avoid decomposition.[3] Prior to use for molecular imprinting the Cu (II) metal-chelate monomer was prepared by the addition of methacryloyl benzotriazole (0.5 g, 2.7 mmol) into 20 mL of ethanol, followed by the addition of $Cu(NO_3)_2{\cdot}3H_2O$ copper nitrate (0.65 g, 2.7 mmol) at room temperature. The solution allowed to be stirred for 3 h and then the solvent was evaporated under vacuum. The complex was recrystallized from ethanol:acetonitrile (20:80).

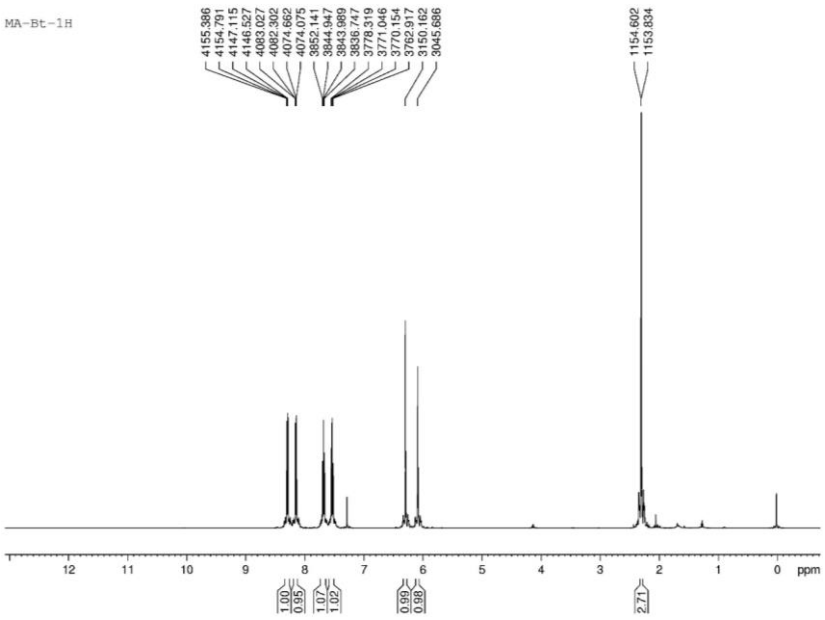

Fig. S4 ^{1}H-NMR spectrum of methacryloyl benzotriazole functional monomer. ^{1}H-NMR (500 MHz, $CHCl_3$-d) δ: 8.23 (d, 1H, Ar-*H*, J=8.2Hz), 8.09 (d, 1H, Ar-*H*, J=8.2Hz), 7.62 (t, 1H, Ar-*H*, J=8.20, 15.40Hz), 7.49 (t,1H, Ar-*H*, J=8.20, 16.38Hz), 6.26 (s, 1H, CH_2=C(CH_3)-), 6.05 (d, 1H, CH_2=C(CH_3)-, J=1.52Hz), 2.45 (s, 3H, -CH_3).

1.3 Synthesis of *N*-methacryloyl-(*L*)-histidine methylester for FM6

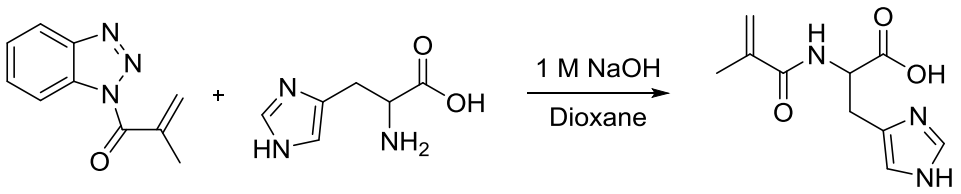

Fig. S5 Synthesis of methacryloyl-(*L*)-histidinemethylester using methacryloyl benzotriazole, (*L*)-histidine in dioxane:water (50:50).

(*L*)-histidine amino acid (1 g, 6.44 mmol) was dissolved in equimolar amount of aqueous 1 M NaOH. A solution of methacryloyl benzotriazole (1.21 g, 6.44 mmol) in 15 mL of 1,4-dioxane was added dropwise to the amino acid solution. The reaction mixture was allowed to stir for 30 min at room temperature, after which the 1,4-dioxane was evaporated under vacuum. The residue was diluted with 50 mL water and extracted with ethyl acetate (3x 60 mL) to remove 1H-benzotriazole. The collected aqueous phase was neutralized to pH=6.5 using 100 mM HCl. The pH needs to be carefully monitored and kept around 6–7 to prevent possible polymerization of methacryloyl group in acidic medium. Water was removed under vacuum to give the monomer in 90 % yield. Prior to use for molecular imprinting the Cu (II) metal-chelate monomer was prepared by the addition of methacryloyl-(*L*)-histidinemethylester (0.51 g, 2.2 mmol) into 20 mL of deionized water, followed by the addition of $Cu(NO_3)_2 \cdot 3H_2O$ copper nitrate (0.53 g, 2.2 mmol) at room temperature. The solution allowed to be stirred for 3 h while it turned clear blue. The complex was recrystallized from ethanol:acetonitrile (20:80).

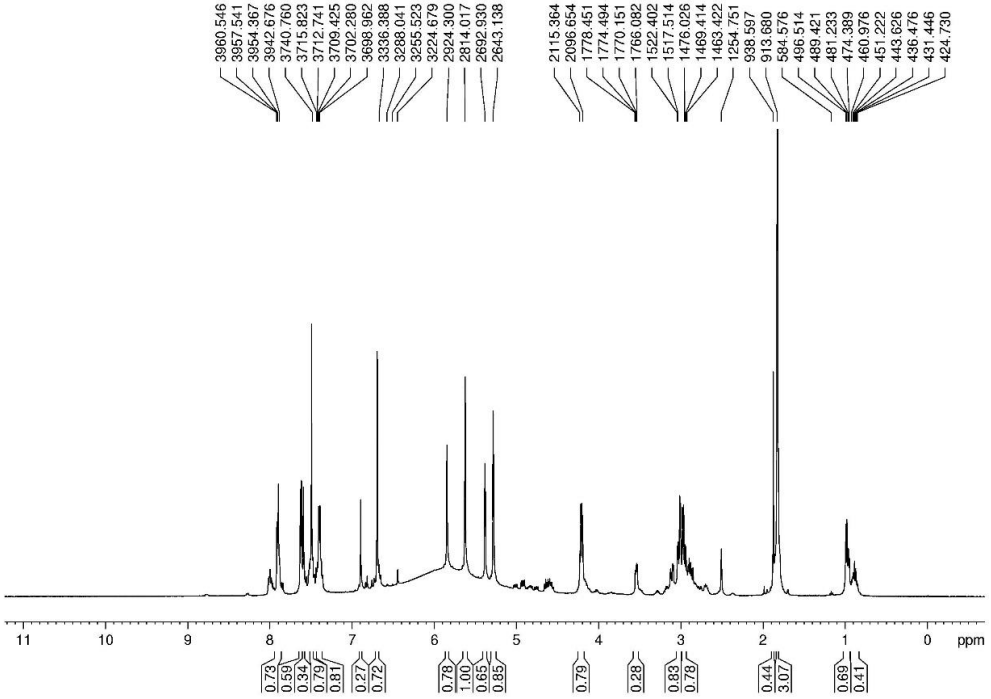

Fig. S6 ^{1}H-NMR spectrum of methacryloyl benzotriazole functional monomer. ^{1}H-NMR (500 MHz, DMSO-d6) δ: 7.90 (s, 1H, N-H), 7.60 (d, 1H, Ar-H, J=5.40 Hz), 7.40 (d, 1H, Ar-H, J=5.40 Hz), 6.85 (s, 1H, NH), 5.82 (s, 1H, CH_2=C(CH_3)-), 5.60 (s, 1H, CH_2=C(CH_3)-), 4.2 (dd, 1H, HOCH_2- CH-NH), 3.0 (m, 2H, HOCH_2-CH-NH), 1.80 (s, 3H, CH_3).

2. Preparation of Imprinted Polymers

MIP microspheres were prepared by a suspension polymerization method according to our reported procedure.[4] Briefly, in a typical MIP fabrication procedure the methacrylic acid functional monomer (1 mmol), oleuropein template (1 mmol), EDMA cross-linker (15 mmol), AIBN initiator (0.1 wt%), perfluoro polymeric surfactant (PFPS) emulsifier (75 mg), perfluoro methylcyclohexane (PMC) dispersing phase (60 mL) and acetonitrile porogen (15 mL) were stirred at 300 rpm. The imprinted polymers were obtained by polymerization involving irradiation of the stirred mixture with UV light for 6 hours at a wavelength of 365 nm at room temperature under an inert Nitrogen atmosphere. The resulting beads were filtered and the remaining template and unreacted molecules were extracted by sequential washing with methanol. The MIPs were dried under reduced pressure for 24 h at room temperature.

Table S1. Stoichiometry of the oleuropein imprinted polymers. The corresponding control polymers (CP1–CP11) were prepared under the same conditions but in the absence of the template. Oleuropein (OR) was used as template, ethylene glycol dimethacrylate was employed as crosslinker (CL), while methacrylic acid (FM1), acrylamide (FM2), 1-(4-vinylphenyl)-3-(3,5-bis(trifluoromethyl)phenyl)urea (FM3), styrene (FM4), methacryloyl benzotriazole–Cu(II) metal-chelate (FM5), and *N*-methacryloyl-(*L*)-histidine methylester–Cu(II) metal-chelate (FM6) were used as functional monomers. See Fig. 3 in the main text for the chemical structures.

Polymer (-)	Stoichiometry (mol/mol/mol)	Theoretical adsorption capacity (μmol OR / g polymer)
IP1	OR/FM1/CL (1/1/15)	327
IP2	OR/FM2/CL (1/1/15)	328
IP3	OR/FM3/CL (1/1/15)	299
IP4	OR/FM1/CL (1/2/15)	318
IP5	OR/FM2/CL (1/2/15)	321
IP6	OR/FM3/CL (1/2/15)	269
IP7	OR/FM1/FM4/CL (1/2/1/15)	308
IP8	OR/FM2/FM4/CL (1/2/1/15)	311
IP9	OR/FM3/FM4/CL (1/2/1/15)	261
IP10	OR/FM5/CL (1/2/15)	259
IP11	OR/FM6/CL (1/2/15)	264

Table S2. Elemental analysis of the imprinted and control polymers after template extraction. Anal. Calcd/Found. Elemental microanalysis of the polymers after extraction confirmed (i) the stoichiometric incorporation of monomers into the polymers, and (ii) the successful removal of the template from the polymers.

Polymers	Carbon (%)	Hydrogen (%)	Nitrogen (%)	Fluorine (%)
IP1	60.47/60.51	7.12/7.14	0.02/0.03	n.a.*
IP2	60.37/60.39	7.12/7.09	0.48/0.51	n.a.
IP3	59.93/59.96	6.69/6.67	0.85/0.87	3.40/3.38
IP4	60.34/60.34	7.12/7.15	0.02/0.02	n.a.
IP5	60.15/60.18	7.12/7.11	0.94/0.96	n.a.
IP6	59.39/59.35	6.34/6.37	1.52/1.49	6.12/6.09
IP7	61.36/61.37	7.14/7.15	0.02/0.03	n.a.
IP8	61.19/61.17	7.14/7.16	0.89/0.87	n.a.
IP9	60.28/60.31	6.38/6.38	1.48/1.45	5.95/5.91
IP10	61.00/61.04	6.87/6.84	2.53/2.56	n.a.
IP11	59.72/59.75	6.96/6.98	2.47/2.50	n.a.
CP1	60.47/60.42	7.12/7.14	0.02/0.00	n.a.
CP2	60.37/60.41	7.12/7.10	0.48/0.45	n.a.
CP3	59.93/59.91	6.69/6.66	0.85/0.84	3.40/3.37
CP4	60.34/60.35	7.12/7.09	0.02/0.03	n.a.
CP5	60.15/60.17	7.12/7.13	0.94/0.97	n.a.
CP6	59.39/59.44	6.34/6.35	1.52/1.53	6.12/6.11
CP7	61.36/61.35	7.14/7.12	0.02/0.02	n.a.
CP8	61.19/61.24	7.14/7.11	0.89/0.85	n.a.
CP9	60.28/60.25	6.38/6.39	1.48/1.46	5.95/5.93
CP10	61.00/59.95	6.87/6.85	2.53/2.49	n.a.
CP11	59.72/59.76	6.96/6.93	2.47/2.51	n.a.

*n.a. = not applicable

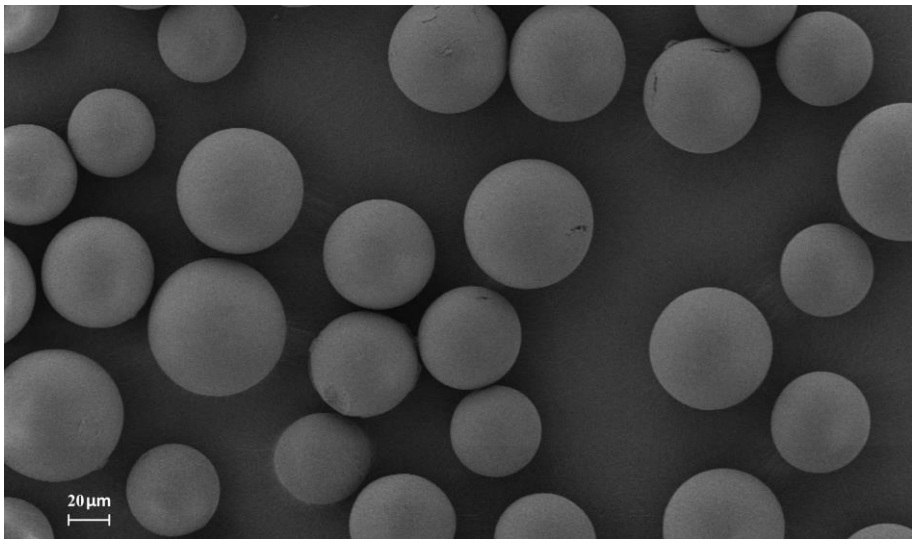

Fig. S7 Typical scanning electron micrographs (SEM) of MIP7 imprinted polymer at 600x magnification. The particles are spherical, uniformly sized with a size range of 45−70 µm, which is suitable for chromatographic stationary phase and solid-phase extraction.

3. Screening of Imprinted Polymers

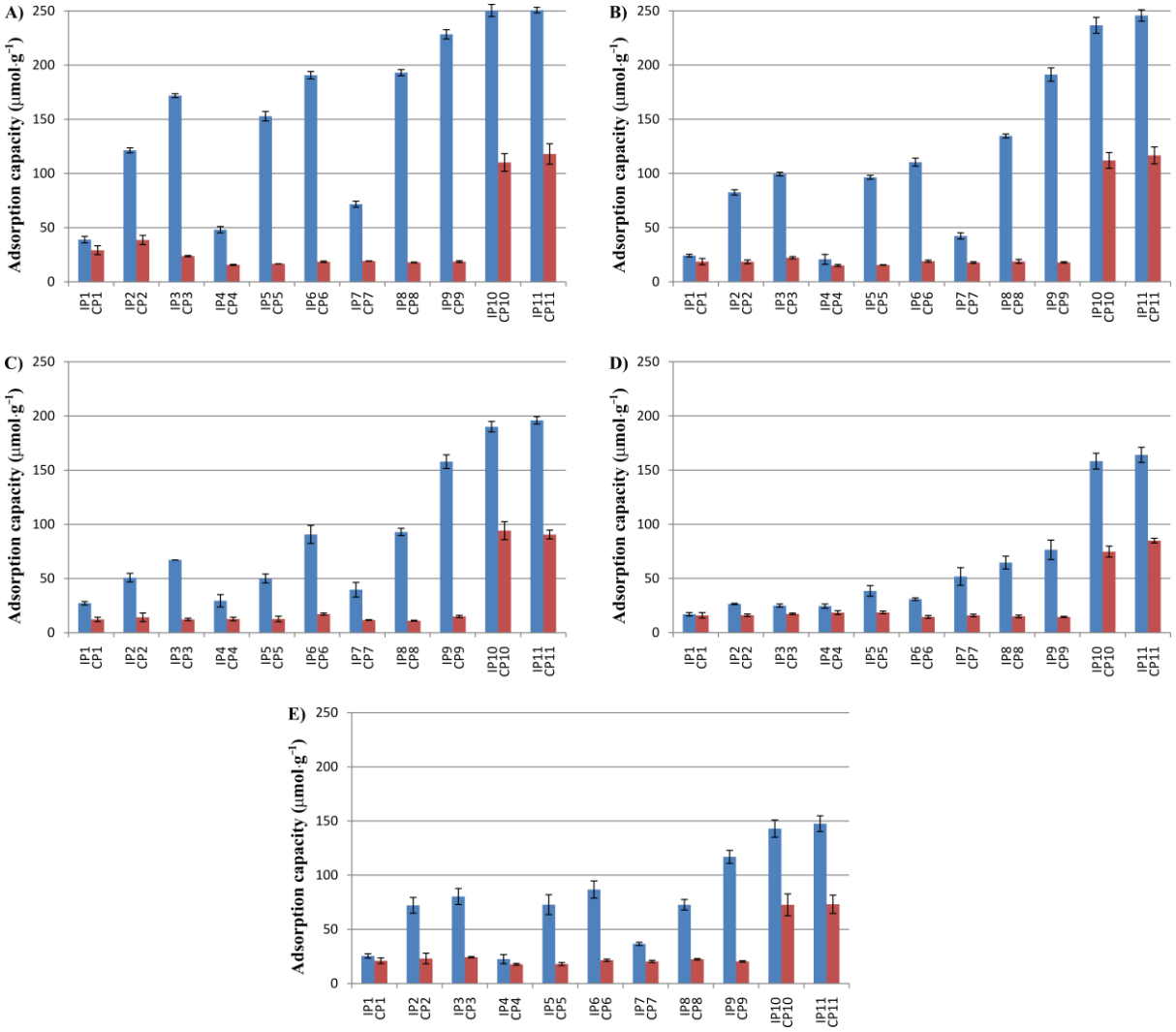

Fig. S8 Screening of solvents and polymers through adsorption capacity: **A**) ethyl acetate, **B**) cyclohexanone, **C**) sulfolane, **D**) isopropyl alcohol, and **E**) 1,2-propanediol. IP1–CP11 are the imprinted polymers, and CP1–CP11 are the corresponding control polymers. The reproducibility is demonstrated through the error bars based on 3–5 adsorption–desorption cycles using two independently prepared polymers. The adsorption capacity is expressed as µmol oleuropein per gram of adsorbent. The adsorbent mass to system volume ratio was fixed at 5 $g \cdot L^{-1}$.

4. Adsorption Column Dynamics

A mathematical model has been developed to describe the dynamics of the adsorption process. The model is based on mass and heat balances to the flowing liquid and stationary solid phase in the adsorption column. The following assumptions have been considered: no gradients of velocity, concentration and temperature in the radial direction of the column; homogeneous bed porosity in the entire domain; external mass transfer resistance to the polymer particles described by the film resistance theory; axial mass dispersion in the porous bed. With the above-mentioned assumptions, the differential mass balance to the liquid phase has the form

$$\varepsilon\frac{\partial C}{\partial t}+\varepsilon\frac{\partial}{\partial x}\left(u\frac{\partial C}{\partial x}-D_{\mathrm{L}}\frac{\partial C}{\partial x}\right)=-(1-\varepsilon)k_{\mathrm{film}}\frac{6}{d_{\mathrm{p}}}\left(C-C_{\mathrm{S}}\right) \qquad \text{Eq. S1}$$

where x is the axial position in the column, t the flow time, ε the packed bed porosity, C the concentration of oleuropein in the liquid phase, C_{S} the concentration at the surface of the polymer particles, k_{film} the mass transfer coefficient in the film of stagnant fluid surrounding the polymer particles, d_{p} the average diameter of the particles and D_{L} the longitudinal dispersion coefficient. The interstitial velocity, u, is defined as

$$u\equiv\frac{U}{\varepsilon}=\frac{4Q}{\pi D^{2}\varepsilon} \qquad \text{Eq. S2}$$

where U is the superficial velocity, Q is the volumetric flow rate and D the column internal diameter.

The Linear Driving Force (LDF) model proposed by Glueckauf and Coates[5] has been adopted in the mass balance to the solute in the solid phase for its simplicity, allowing to reduce considerably the computational time, while being physically consistent[6]. The differential mass balance to the volume-averaged concentration of the solute adsorbed in the polymer particles, $\langle q\rangle$, is given by

$$\frac{\partial\langle q\rangle}{\partial t}=\frac{15D_{\mathrm{eff}}(T)}{d_{p}^{2}/4}\left(q_{\mathrm{eq}}(C_{\mathrm{S}},T)-\langle q\rangle\right) \qquad \text{Eq. S3}$$

where D_{eff} is the effective mass diffusivity inside the pores of the polymer particles and T the temperature. D_{eff} considers the effect of the pores tortuosity and porosity on the transport of the oleuropein molecules inside the polymer particles. The adsorbed solute concentration in equilibrium, q_{eq}, is given by a Langmuir-type expression

$$q_{\mathrm{eq}}(C,T)=q_{\mathrm{max}}\frac{K_{\mathrm{L}}(T)\,C}{1+K_{\mathrm{L}}(T)\,C} \qquad \text{Eq. S4}$$

where q_{max} is the maximum solute adsorbing capacity of the particles and K_{L} the Langmuir model constant. The following closure expression obtained by matching mass fluxes at the surface of the polymer spheres is required to solve the mass balances to the liquid and solid phases (Eq. S1 and S3)

$$(1-\varepsilon)k_{\text{film}}\frac{6}{d_p}\left(C-C_S\right)=(1-\varepsilon)\rho_{\text{app}}\frac{15D_{\text{eff}}}{d_p^2/4}\left(q_{\text{eq}}(C_S,T)-\langle q\rangle\right) \qquad \text{Eq. S5}$$

where ρ_{app} is the apparent density of the dry particles.

The film mass transfer resistance has been estimated from the Ranz-Marshal correlation for mass transfer in flows around spheres

$$\text{Sh}\equiv\frac{k_{\text{film}}d_{\text{p}}}{D_{\text{m}}}=2+1.8\,\text{Re}_{\text{p}}^{1/2}\,\text{Sc}^{1/3} \qquad \text{Eq. S6}$$

where D_{m} is the molecular diffusivity, Sh the Sherwood number, $\text{Re}_{\text{p}}\equiv\varepsilon u d_{\text{p}}/\nu$ is the Reynolds number based on the diameter of the particles and $\text{Sc}\equiv\nu/D_{\text{m}}$ is the Schmidt number. $\nu\equiv\mu/\rho_{\text{liquid}}$ is the liquid kinematic viscosity.

The longitudinal dispersion coefficient in the porous medium, D_{L}, has been estimated by the correlation proposed by Guedes de Carvalho and Delgado[7]

$$\text{Pe}_{\text{L}}\equiv\frac{u d_{\text{p}}}{D_{\text{L}}}=\left(\frac{\text{Pe}_{\text{m}}}{5}(1-p)^2+\frac{\text{Pe}_{\text{m}}^2}{25}p(1-p)^3\left(\exp\left(-\frac{5}{p(1-p)\text{Pe}_{\text{m}}}\right)-1\right)+\frac{1}{\sqrt{2}\text{Pe}_{\text{m}}}\right)^{-1} \qquad \text{Eq. S7}$$

with

$$p=\frac{0.48}{\text{Sc}^{0.15}}+\left(\frac{1}{2}-\frac{0.48}{\text{Sc}^{0.15}}\right)\exp\left(-\frac{75\text{Sc}}{\text{Pe}_{\text{m}}}\right) \qquad \text{Eq. S8}$$

where Pe_{L} and $\text{Pe}_{\text{m}}\equiv u d_{\text{p}}/D_{\text{m}}$ are the longitudinal and molecular Peclet numbers, respectively.

The dynamics of the evolution of the temperature inside the column has been obtained from a global energy balance, assuming unidirectional transport of heat with local instantaneous equilibrium between the temperatures of the liquid and solid phases,

$$\left(\varepsilon\rho_{\text{liquid}}+(1-\varepsilon)\rho_{\text{solid}}\right)C_{\text{p,mix}}\frac{\partial T}{\partial t}+\frac{\partial}{\partial x}\left(\rho_{\text{liquid}}C_{\text{p,liquid}}u-\lambda_{\text{mix}}\frac{\partial T}{\partial x}\right)=0 \qquad \text{Eq. S9}$$

where the overall heat capacity coefficient, $C_{\text{p,mix}}$, is given by

$$C_{\text{p,mix}}=\frac{\left(1-\varepsilon\right)\rho_{\text{solid}}C_{\text{p,solid}}+\varepsilon\rho_{\text{liquid}}C_{\text{p,liquid}}}{\left(1-\varepsilon\right)\rho_{\text{solid}}+\varepsilon\rho_{\text{liquid}}} \qquad \text{Eq. S10}$$

and ρ_{solid} being the density of the liquid-impregnated polymer particles, ρ_{liquid} the density of the liquid, and $C_{\text{p,solid}}$ and $C_{\text{p,liquid}}$ the heat capacity of the solid and liquid phases, respectively. Assuming that heat conduction takes place in series, with heat being transported simultaneously through the liquid and the solid, the overall heat conductivity, λ_{mix}, is given by

$$\frac{1}{\lambda_{\text{mix}}}=\frac{1-\varepsilon}{\lambda_{\text{solid}}}+\frac{\varepsilon}{\lambda_{\text{liquid}}} \qquad \text{Eq. S11}$$

where λ_{solid} and λ_{liquid} are the heat conductivity of the solid particles and the liquid, respectively. Thermal dispersion in the liquid phase due to advective mechanisms, i.e. due to local advective mixing at the bed pore scale, has been neglected.

The differential mass and energy balances describing the column concentration and temperature dynamics have been solved for the boundary conditions summarized in Table S3. The physical quantities used in the simulations are summarized in Table S4.

Table S3. Boundary conditions set for solving the mass and energy balances that describe the dynamics of the adsorption process.

	Inlet $(x=0)$	Outlet $(x=L)$
Eq. S1	$uC_{\text{inlet}}=uC(0,t)-D_L\left.\frac{\partial C}{\partial x}\right\|_{0,t}$	$\left.\frac{\partial C}{\partial x}\right\|_{L,t}=0$
Eq. S9	$u\rho_{\text{liquid}}C_{\text{p,liquid}}T_{\text{inlet}}=u\rho_{\text{liquid}}C_{\text{p,liquid}}T(0,t)-\lambda_{\text{mix}}\left.\frac{\partial T}{\partial x}\right\|_{0,t}$	$\left.\frac{\partial T}{\partial x}\right\|_{L,t}=0$

Table S4. Physical properties of the fluids and packed bed used in the simulations of the adsorption column dynamics.

ε	36%
d_p	60 µm
ρ_{app}	645.5 kg/m^3
D_{m}	1×10^{-9} m^2/s
ρ_{liquid}	894.5 kg/m^3
μ	$1.391\times10^{-5}\exp\left(\frac{1.018\times10^{-3}}{T(^\circ\text{C})+273.15}\right)(\text{Pa}\cdot\text{s})$

The concentration in oleuropein in the feeding stream, C_{inlet}, and its temperature, T_{inlet}, in the boundary conditions of Table S3 have been set to assume different values according to the operation being performed at the time: adsorption, cleaning or desorption. The calculations have been initialized each time with $C(x,0)=\langle q\rangle_{(x,0)}=0$ g/L and $T=25$ °C, for $t=0\ \ \forall x\in[0,L]$.

The mass and energy balance equations have been solved numerically with the finite differences function *pdpe* of MATLAB® 2015a for solving initial-boundary conditions problems for parabolic-elliptic PDEs in 1-D. The time integration has been performed with the ODE15S algorithm for stiff differential equations. Different numbers of divisions in the *x*-direction have been tested to obtain a solution independent of the level of spatial discretization.

5. Adsorption Isotherm Expression

The adsorption process model requires a mathematical expression for the equilibrium isotherm that is both a function of the concentration of oleuropein and the temperature (see Eq. S4). This expression has been obtained from nonlinear regression analysis of experimental data of q_{eq} *vs. C* in equilibrium at different temperatures ranging from 15 °C to 50 °C. The maximum oleuropein adsorbing capacity of the polymer particles, q_{max}, has been assumed to be constant, i.e., independent of the temperature and concentration. For convenience, an expression of the type

$$K_L(T) = \frac{a}{2}\left(1 - \mathrm{erf}\left(\frac{T-b}{c}\right)\right) \qquad \text{Eq. S12}$$

where a, b and c are fitting parameters, has been chosen to describe dependence of the Langmuir model constant, K_L, with temperature. Fig. 5A shows the experimental data obtained for the equilibrium isotherm and the fitting curves. The following parameters have been obtained for a coefficient of determination $R^2 = 0.9989$: $q_{max} = 0.8991$ kg/kg; $a = 0.5870$ m^3/kg; $b = 29.49$ °C; $c = 11.57$ °C.

6. Effective Intra-particular Diffusivity Estimation

The simulation of the transport of oleuropein molecules inside the polymer particles using the LDF model, requires an estimation of the effective intra-particular mass diffusivity. In this work, this value has been obtained from adsorption kinetics experiments described in Section 4.3. Since the adsorption occurs in a vigorously agitated system, spatial gradients of concentration and film resistance can be neglected. Following those assumptions, Eq. S1 and S3 simplify to

$$\frac{\mathrm{d}C}{\mathrm{d}t} = -\frac{1-\varepsilon}{\varepsilon}\rho_{\mathrm{app}}\frac{\mathrm{d}\langle q\rangle}{\mathrm{d}t} \qquad \text{Eq. S13}$$

and

$$\frac{\mathrm{d}\langle q\rangle}{\mathrm{d}t} = \frac{15D_{\mathrm{eff}}}{d_{\mathrm{p}}^2/4}\left(q_{\mathrm{eq}}(C)-\langle q\rangle\right) \qquad \text{Eq. S14}$$

respectively, where D_{eff} is the only unknown parameter that can be obtained by fitting to experimental data. Eq 14 and 15 have been solved for different values of D_{eff} until the summation of the square of the residues between experiments and the model was minimized. Fig. 5B shows the experimental data obtained from the adsorption kinetics experiments at a constant temperature of 25 °C and the model with the fitted value of the intra-particular effective diffusivity. A value of $D_{\mathrm{eff}} = 1.07\times10^{-14}$ m^2/s for a coefficient of determination $R^2 = 0.983$ has been obtained.

The Stokes-Einstein relation

$$\frac{D_{\mathrm{eff}}(T)}{D_{\mathrm{eff}}(T_{\mathrm{ref}})} \approx \frac{D_{\mathrm{m}}(T)}{D_{\mathrm{m}}(T_{\mathrm{ref}})} = \frac{\mu(T_{\mathrm{ref}})}{\mu(T)}\frac{T+273.15}{T_{\mathrm{ref}}+273.15} \qquad \text{Eq. S15}$$

has been adopted to estimate D_{eff} for any given temperature, T, other than the reference temperature $T_{\mathrm{ref}} = 25$ °C, This assumes that the polymer particles' tortuosity and porosity do not change significantly within the temperature range of the experiments.

7. Membrane Separation System

The nanofiltration rig shown in Fig. S9 was used to obtain rejection and flux data (Fig. S10) for the oleuropein solution. GMT-oNF-1® and GMT-oNF-2® (purchased from Borsig GmbH), NF010306 and NF030306 (purchased from SolSep BV), as well as 26PBI (in-house fabricated 26 wt% polybenzimidazole membranes based on Livingston *et al.*[8]) solvent-resistant nanofiltration membranes were tested at 10–40 bar using either crude oleuropein solution obtained from the olive leaf digestion process or purified oleuropein solution collected from the adsorbent column.

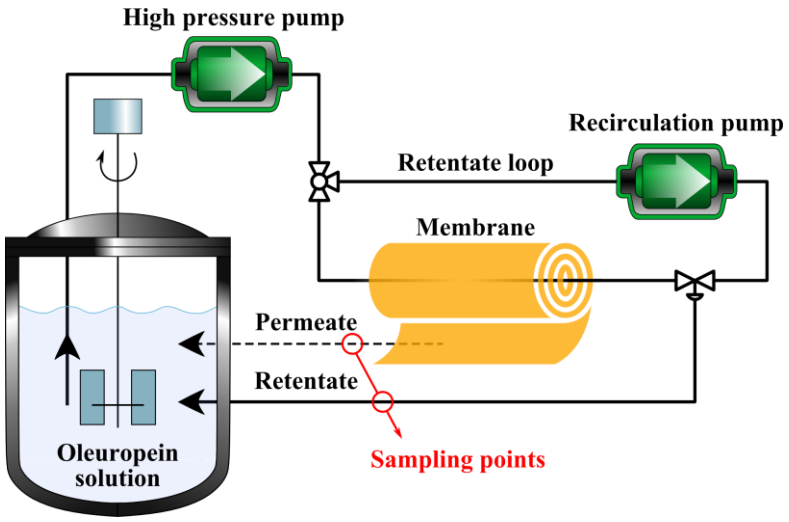

Fig. S9 Schematic process configuration for initial data acquisition, i.e. determination of solute rejection and flux on different membranes at 10–40 bar pressure.

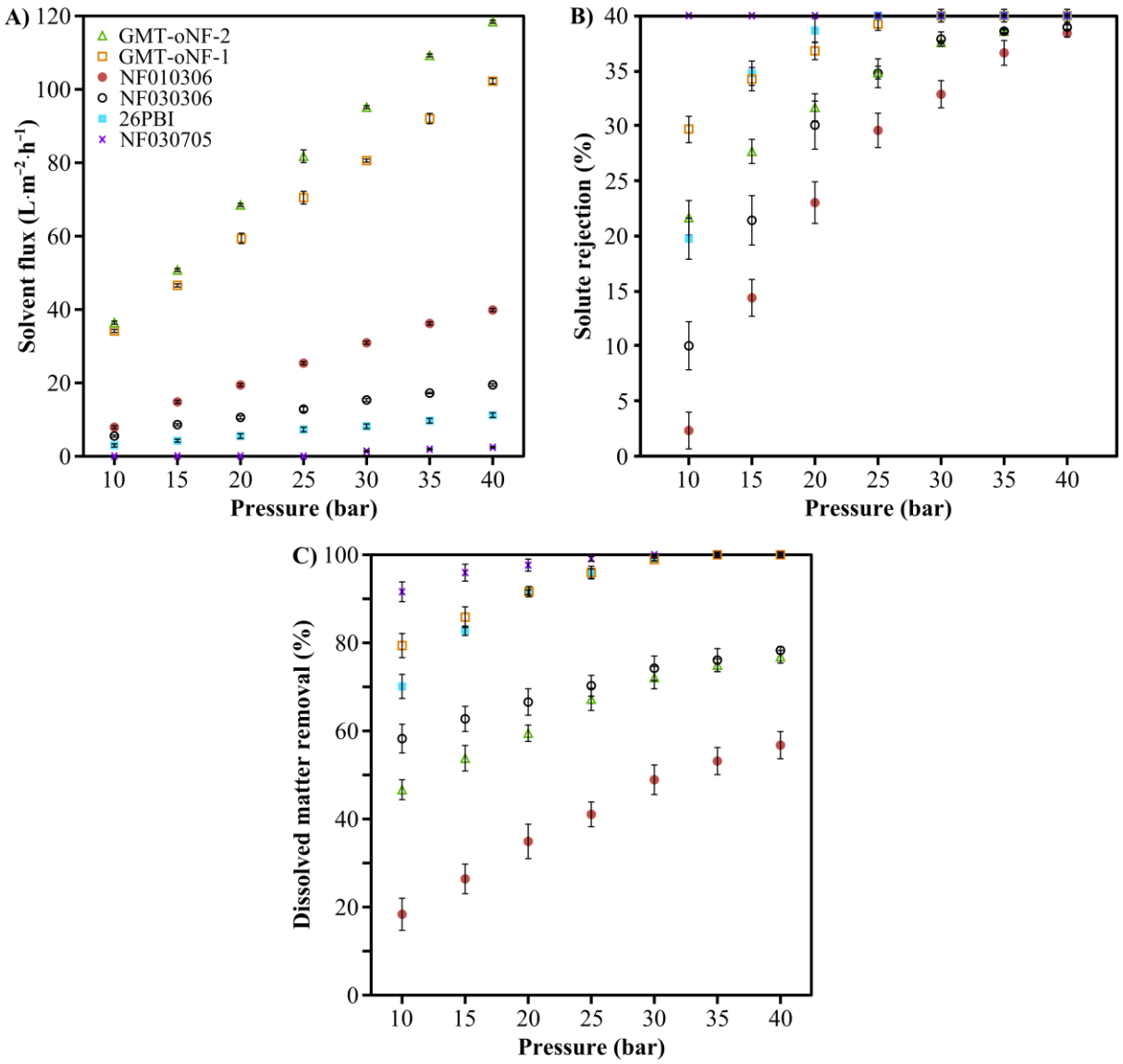

Fig. S10 Membrane screening at various pressure for the comparison of solvent flux (**A**), solute rejection for the concentration of oleuropein prior to crystallization (**B**) and removal of dissolved matter from the waste stream (**C**).

The dynamics of the oleuropein concentration in the membrane cell, C_{memb}, can be described by the ordinary differential equation

$$\frac{\mathrm{d}C_{\text{memb}}}{\mathrm{d}t} = \frac{Q}{V_{\text{memb}}}\left(C(L,t) - \alpha C_{\text{memb}}\right) \qquad \text{Eq. S16}$$

where it has been assumed the absence of spatial gradients of concentration in the membrane cell volume, V_{memb}, due to strong mixing induced by the recirculation circuit. $C(L,t)$ is the concentration of oleuropein at the outlet of the adsorption column. α is the fraction of the total volumetric flow rate, Q, that is being extracted continuously from the membrane cell volume. The solvent is being recovered at a flow rate equal to $(1-\alpha)Q$.

8. Hybrid Process Simulation

As indicated in Section 2.2 of the main manuscript, a parametric study has been done in order to define a suitable threshold concentration, $C_{threshold}$, measured at the outlet of the column that, when reached, determines the end of the adsorption step. This concentration should be appropriately chosen in order to avoid the waste of oleuropein and to optimizing the usage of the total adsorption column capacity. The total processed mass of oleuropein, i.e. the total mass fed to the adsorption column, is given by

$$m_{processed} = V_{processed} C_{inlet} \qquad \text{Eq. S17}$$

where the total volume of processed solution, $V_{processed}$, was chosen so that $C(V_{processed}) = C_{threshold}$ and C_{inlet} is the concentration of the solution fed to the column. From the breakthrough curve, the mass of oleuropein that is lost, m_{lost}, and the mass that is recovered, $m_{recovered}$ can be calculated as

$$m_{lost} = \int_0^{V_{processed}} C(V)\,dV \qquad \text{Eq. S18}$$

and

$$m_{recovered} = \int_0^{V_{processed}} \left(C_{inlet} - C(V)\right) dV \qquad \text{Eq. S19}$$

respectively. For clarity, Fig. S11 shows the geometrical interpretation of m_{lost} and $m_{recovered}$ in the breakthrough curve plot. The effect of changing the value of $C_{threshold}$ on the used column adsorption capacity and the ratio between the lost and total processed oleuropein mass can be seen in Fig. 6B and 6C in the main article.

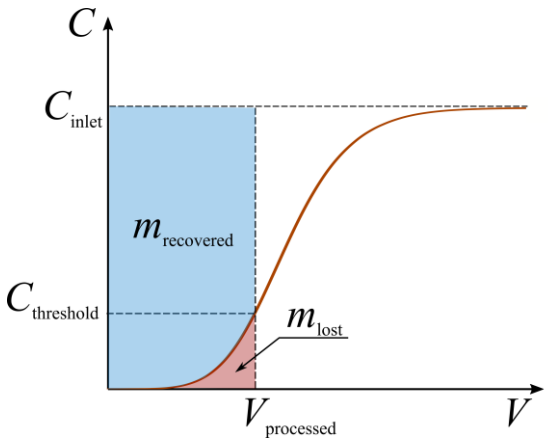

Fig. S11 Breakthrough curve of the adsorption process with the geometrical interpretation of the recovered and lost mass as a function of the threshold concentration.

To simulate the full oleuropein recovery process, the concentration of oleuropein, C_{inlet}, and the temperature, T_{inlet}, of the feeding stream has been set according to each step of the process, as summarized in Table S5. t_{ads} is the time necessary during the adsorption step so that the defined

threshold concentration of 50 ppm is reached at the column outlet. t_{clean} is the time necessary during a cleaning step to replace the void fraction of the adsorption column with pure solvent after the adsorption step. This cleaning step intends to remove all impurities from the system before the desorption recovery step starts. The value of t_{clean} has been defined as

$$t_{clean} = 1.1\frac{L}{u} \qquad \text{Eq. S20}$$

to ensure that 99.9% of the previous liquid in the column void fraction has been replaced by pure solvent. After the cleaning step, the column and solvent feed are heated until a temperature of 50 °C to promote the oleuropein desorption.

Table S5. Modulation of the inlet concentration and temperature in the full separation process.

Adsorption step	Cleaning step	Heating and desorption steps
for $0 \le t < t_{ads}$	for $t_{ads} \le t < t_{ads} + t_{clean}$	for $t \ge t_{ads} + t_{clean}$
$C_{inlet} = 0.966$ g/L $T_{inlet} = 25$ °C $Q = 2$ mL/min	$C_{inlet} = 0$ g/L $T_{inlet} = 25$ °C $Q = 2$ mL/min	$C_{inlet} = 0$ g/L $T_{inlet} = \min\left(50, 25 + \frac{25}{720}\left(t - t_{ads} - t_{clean}\right)\right)$(°C) $Q = 2$ mL/min

The mass and energy balances describing the dynamics of adsorption of oleuropein in the column have been solved for the inlet conditions in Table S5. Fig. S12 and S13 show, respectively, the simulated concentration of oleuropein in the liquid and adsorbed in the solid as a function of the position in the column and the processed volume.

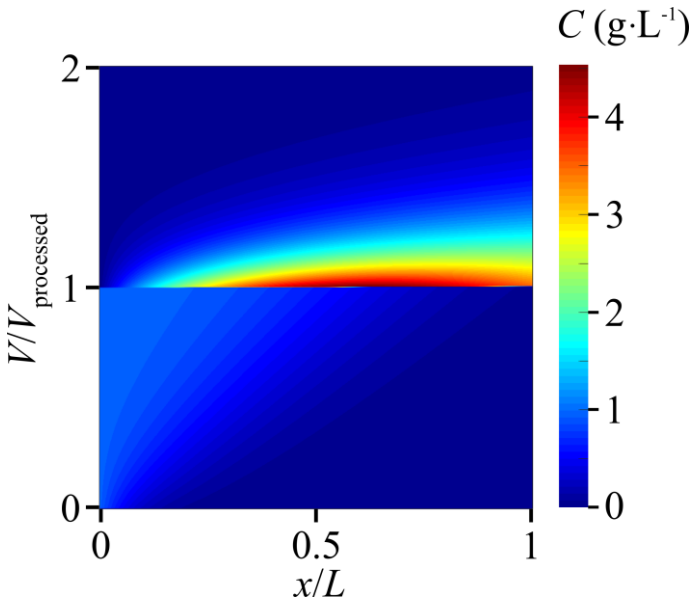

Fig. S12 Concentration of oleuropein in the liquid as a function of the position in the column and the processed volume.

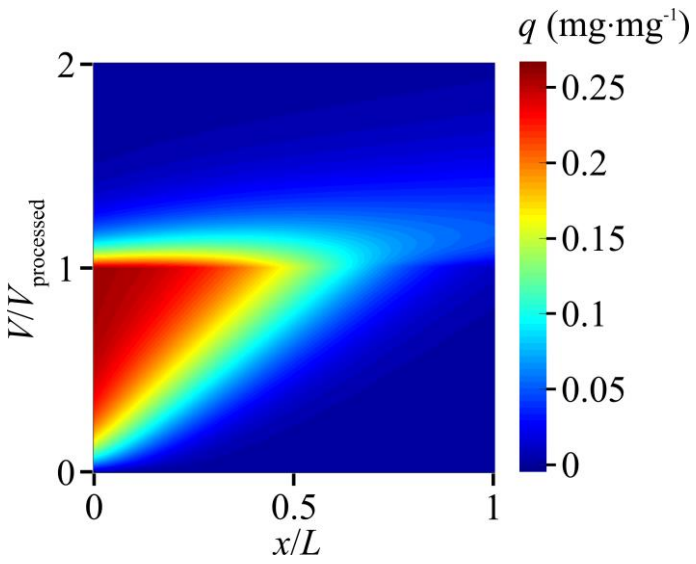

Fig. S13 Concentration of adsorbed oleuropein as a function of the position in the column and the processed volume.

The concentration of oleuropein at the outlet of the adsorption column obtained numerically as a function of the processed volume for one full separation process cycle was compared with experimental values (Fig. S14).

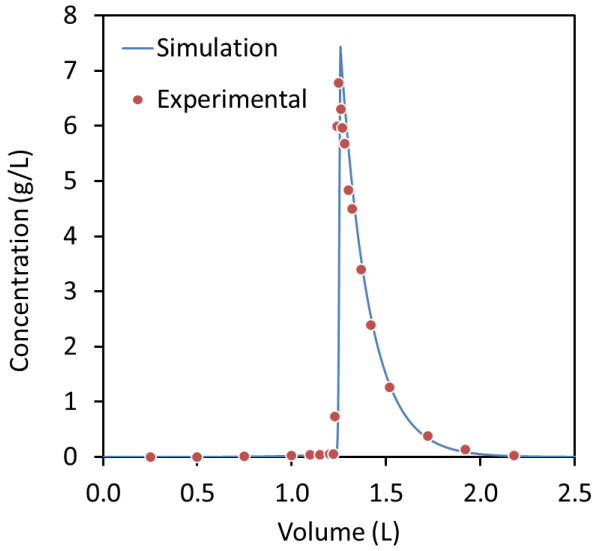

Fig. S14 Concentration of oleuropein at the outlet of the adsorption column as a function of the processed volume for one full separation process cycle.

It can be observed in Fig. S14 that the times for the adsorption and desorption steps are similar when the column is heated up to 50 °C. This suggests that the process can be made continuous if two beds are used simultaneously with automated flow switching valves. The results in Fig. S14 suggest, however, that the desorption step is slightly faster, what leads to solvent waste. In Section 8, a solution is proposed by studying the reduction of the desorption step temperature towards the equalisation of the two steps durations. In addition to avoiding the waste of solvent, the reduction of the maximum process temperature will also be translated into energy savings.

Eq. S16 has also been solved to predict the concentration of oleuropein in the membrane cell. The numerical predictions are compared with experimental results in Fig. S15. Both results in Fig. S14 and Fig. S15 show a quite good agreement between experimental results and the numerical model of the adsorption process dynamics.

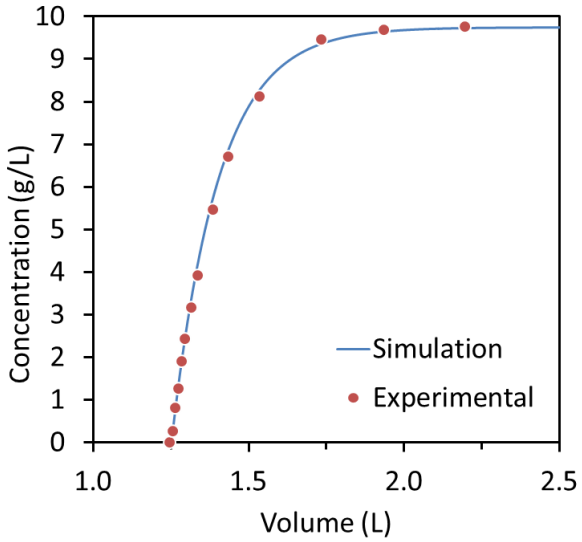

Fig. S15 Concentration of oleuropein in the nanofiltration cell as a function of the processed volume.

9. Continuous Process Design

The developed numerical model of the column dynamics has been used to determine the appropriate temperature to set during the desorption step that allows to obtain equal times for the adsorption and desorption. This has been possible because isotherm equilibrium data has been obtained for different temperatures (see Fig. 5A of the main article). As mentioned in Section S8, this has the advantage to allow the development of a continuous process using only two chromatographic beds, minimizing solvent waste and optimizing energetic requirements. The column inlet conditions set in each step are summarized in Table S6. The temperature of the inlet fluid in the desorption step, T_{desor}, has been varied between 40 °C and 50 °C, with an increment of 2.5 °C. The effect of the desorption temperature on the column's dynamics is shown in Fig. 7A.

Table S6. Modulation of the inlet concentration and temperature in the continuous process.

Adsorption step	**Cleaning step**	**Heating and desorption steps**
for $0 \le t < t_{ads}$	for $t_{ads} \le t < t_{ads} + t_{clean}$	for $t_{ads} + t_{clean} \ge t > 2\left(t_{ads} + t_{clean}\right)$
$C_{inlet} = 0.966$ g/L	$C_{inlet} = 0$ g/L	$C_{inlet} = 0$ g/L
$T_{inlet} = 25$ °C	$T_{inlet} = 25$ °C	$T_{inlet} = T_{desor}\,(°C)$
$Q = 2$ mL/min	$Q = 2$ mL/min	$Q = 2$ mL/min

From the numerical results, a temperature T_{desor} has been chosen to equalise the adsorption and desorption times. These conditions ensure that ~99% of the oleuropein is desorbed from the column during the desorption step. The fully continuous process with two beds has been tested experimentally for four cycles and compared with the numerical predictions (Fig. 7B). It can be seen from Fig. 7B that an excellent agreement between the mathematical model and the experimental results has been obtained. The concentration at the outlet of the two beds system shows a fully periodic evolution with no noticeable degradation in the columns separation performance during the experimental run.

The concentration of oleuropein at the membrane cell volume and in the collecting flask has also been monitored experimentally. For the fully continuous process, a value of $\alpha = 2.5\%$ has been used to ensure that no precipitation of oleuropein would occur in the membrane cell and collection flask. Eq. S16 has also been solved and compared to the experimental results. Fig. 7C shows a good agreement, with minor deviations, between the concentration of oleuropein obtained experimentally and by simulation. It can be observed that at $\alpha = 2.5\%$ the concentration of oleuropein evolves to a state where it continuously fluctuates in the membrane cell around 35 ± 5 g·L^{-1}.

10. Characterisation of the Isolated Oleuropein

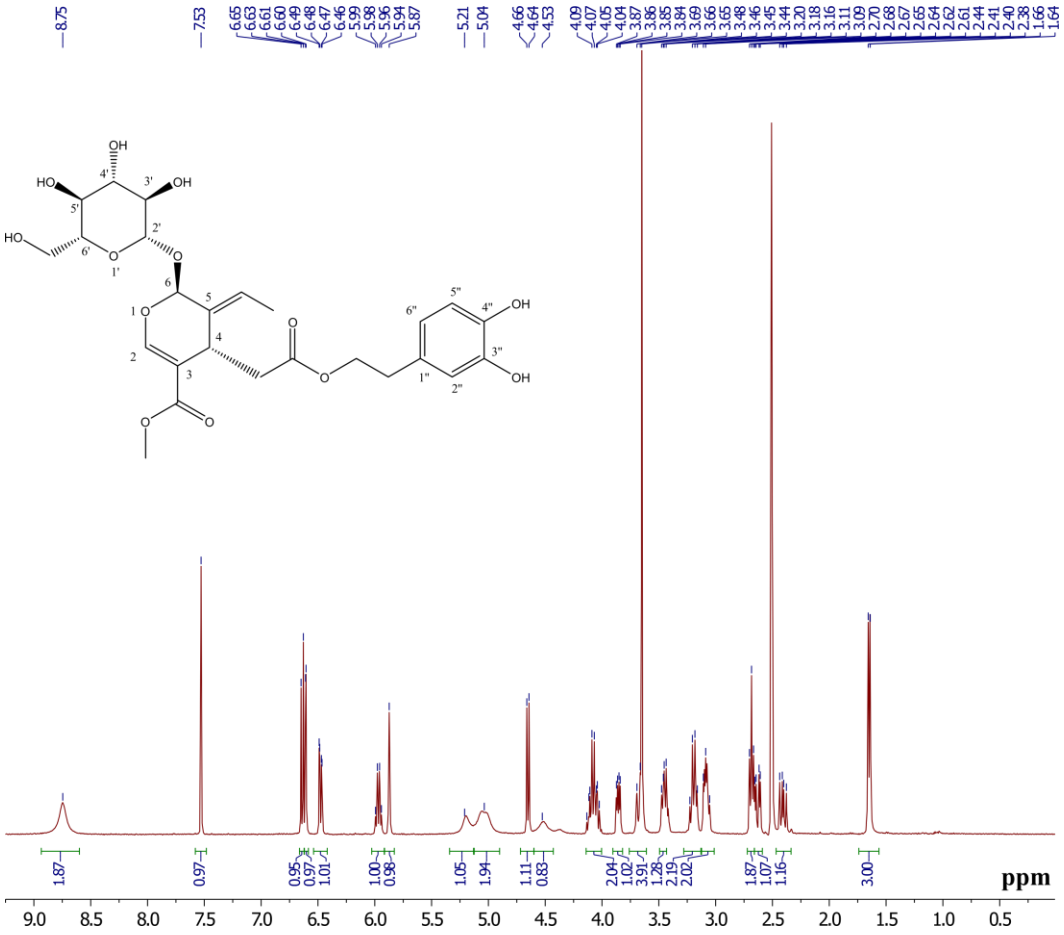

Fig. S16 ^{1}H-NMR spectrum of 1-(4-vinylphenyl)-3-(3,5-bis(trifluoromethyl)phenyl)urea functional monomer. ^{1}H-NMR (400 MHz, DMSO-d_6) δ: 1.63 (3H, dd, *J*=7.0, 1.2 Hz, ethylydene CH_3), 2.41 (1H, dd, *J*=14.6, 9.2 Hz, CH_2COO), 2.63 (1H, dd, *J* = 14.4, 4.4 Hz, CH_2COO), 2.68 (2H, t, *J*=7.2 Hz, ArCH_2), 3.06–3.11 (2H, m, glycosyl CH-3' and CH-5'), 3.16–3.23 (2H, m, glycosyl CH-4' and CH-6'), 3.46 (1H, dd, *J* = 12.0, 6.4 Hz, glycosyl CH-6'-CH_2), 3.65 (3H, s, OCH_3), 3.66–3.69 (1H, m, glycosyl CH-6'-CH_2), 3.86 (1H, dd, *J* = 7.8, 4.2 Hz, pyran CH-4), 4.02–4.13 (2H, m, COOC$H_2$$CH_2$), 4.53 (1H, br. s, glycosyl CH-6'-CH_2O*H*), 4.65 (1H, d, *J*=8.0 Hz, glycosyl CH-2'), 5.04 (2H, br. s, glycosyl 3'-OH and 4'-OH), 5.21 (1H, br. s, glycosyl 5'-OH), 5.87 (1H, s, pyran CH-2), 5.97 (1H, q, *J*=6.4 Hz, ethylydene CH), 6.48 (1H, dd, J_{orto}=8.0 Hz, J_{meta}=2.0 Hz, Ar-CH-6"), 6.61 (1H, d, J_{meta}=2.0 Hz, Ar-CH-2"), 6.64 (1H, d, J_{orto}=8.0 Hz, Ar-CH-5"), 7.53 (1H, s, pyran CH-6), 8.75 (2H, br s, phenolic OHs) ppm.

Fig. S17 ^{13}C-NMR spectrum of 1-(4-vinylphenyl)-3-(3,5-bis(trifluoromethyl)phenyl)urea functional monomer. ^{13}C-NMR (100 MHz, DMSO-d_6) δ: 12.97 (ethylydene CH_3), 30.08 (C-4), 33.65 ($CH_2COOCH_2\underline{C}H_2$), 40.08 ($\underline{C}H_2COOCH_2CH_2$), 51.23 ($OCH_3$), 61.06 (C-6'-$\underline{C}H_2OH$), 65.01 ($CH_2COO\underline{C}H_2CH_2$), 69.88 (C-5'), 73.22 (C-3'), 76.46 (C-6'), 77.32 (C-4'), 92.87 (C-6), 98.94 (C-2'), 107.63 (C-3), 115.47 (C-2"), 116.12 (C-5"), 119.48 (C-6"), 122.99 (ethylydene CH), 128.33 (C-5), 129.08 (C-1"), 143.71 (C-4"), 145.04 (C-3"), 153.39 (C-2), 166.13 ($\underline{C}OOCH_3$), 170.63 ($CH_2\underline{C}OOCH_2CH_2$) ppm.

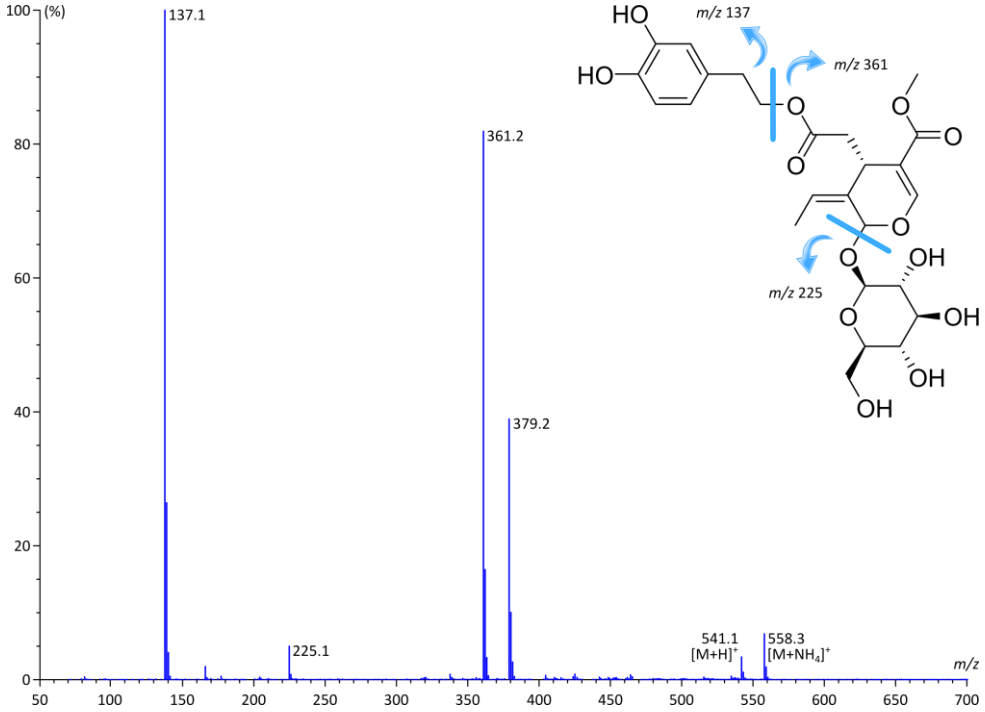

Fig. S18 Mass spectrum of the isolated oleuropein. The main peaks correspond to the fragments reported in the literature.[9]

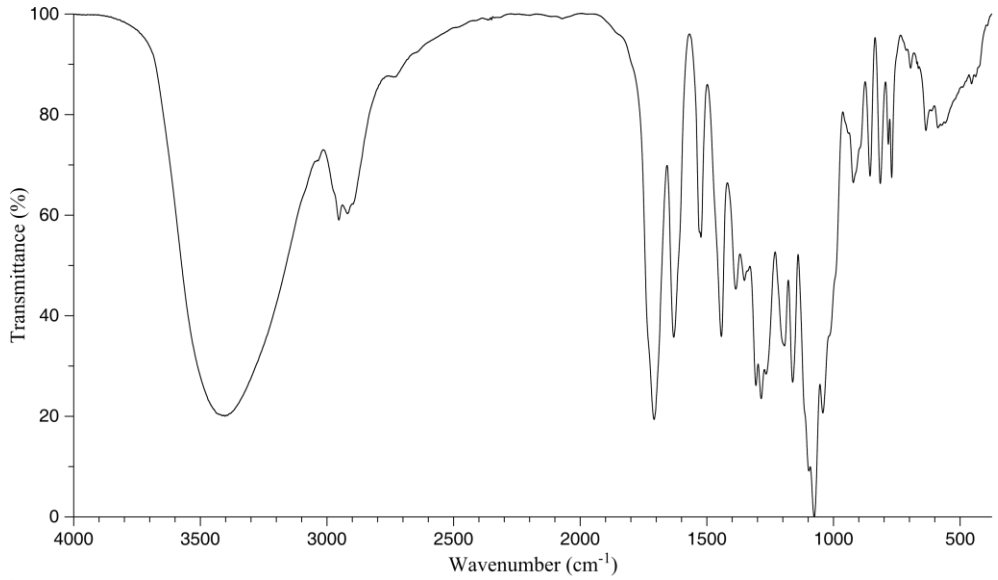

Fig. S19 Infrared (IR) spectrum of the isolated oleuropein which was found to be identical to the reported spectrum in the literature.[10] IR (KBr) ν_{max} 3401 (υ_{O-H}), 2952 ($\upsilon_{C-H,\,s}$), 2918 ($\upsilon_{C-H,\,s}$), 1707 ($\upsilon_{C=O}$), 1630 ($\upsilon_{C=C}$), 1523 ($\upsilon_{C=C,\,in\,ring}$), 1442 ($\delta_{CH3,\,as}$), 1385 ($\beta_{O-H}$), 1351 ($\delta_{CH3,\,s}$), 1306, 1285, 1193, 1161 ($\upsilon_{C-O-C,\,as}$), 1076 ($\upsilon_{C-O-C,\,s}$), 1042, 921, 855, 815 ($\gamma_{=CH}$), 783, 770, 695, 635 cm^{-1}.

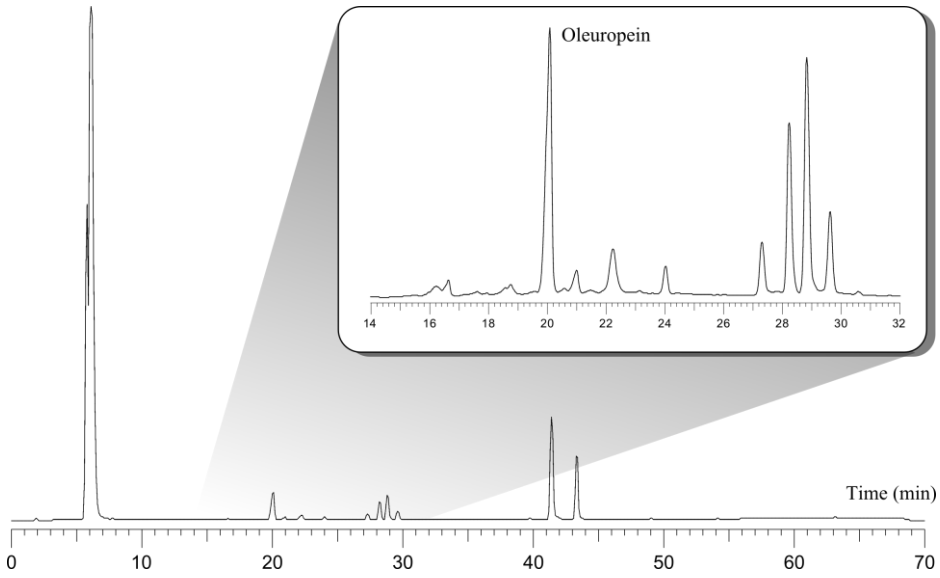

Fig. S20 HPLC chromatogram of the crude oleuropein obtained from the olive leaf digestion process. ACE 5 µm, C18, 100 Å, 150 × 4.6 mm column was used with an eluent flow rate of 1 mL·min^{-1} and UV acquisition at 250 nm. Eluent A was acetonitrile and eluent B was water containing 0.1% trifluoroacetic acid. The gradient was linear from 10 to 90% A in 60 min, followed by 90% A hold for further 5 min and a re-equilibration period of 15 min. The column temperature was 25 °C and the injection volume 15 µL. The retention time for oleuropein was 20 min.

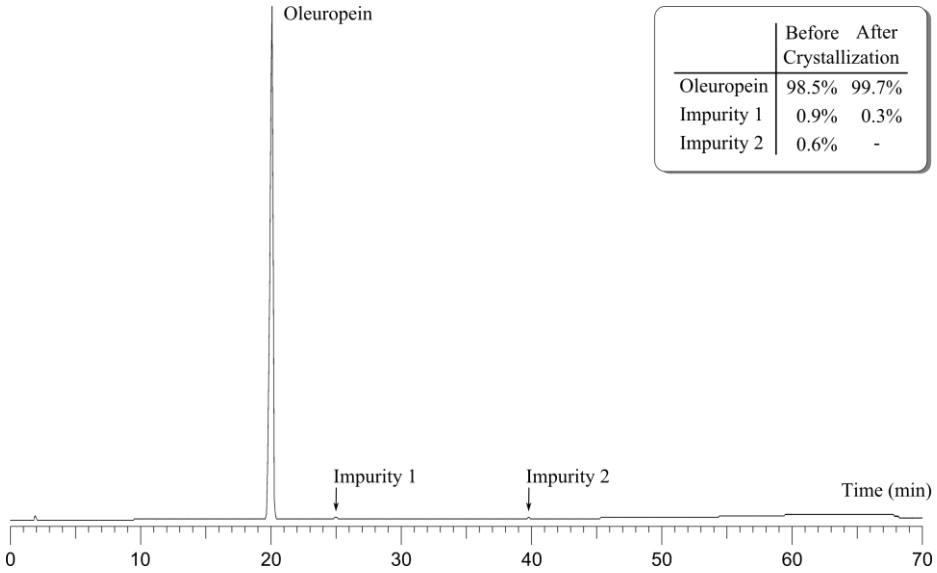

	Before Crystallization	After Crystallization
Oleuropein	98.5%	99.7%
Impurity 1	0.9%	0.3%
Impurity 2	0.6%	-

Fig. S21 HPLC chromatogram of the isolated oleuropein prior to the crystallization step. At this stage the purity of oleuropein was found to be 98.5%, and two minor impurities remained in the product stream at 24.9 and 39.7 min retention time. The crystallization increased the final purity to 99.7%.

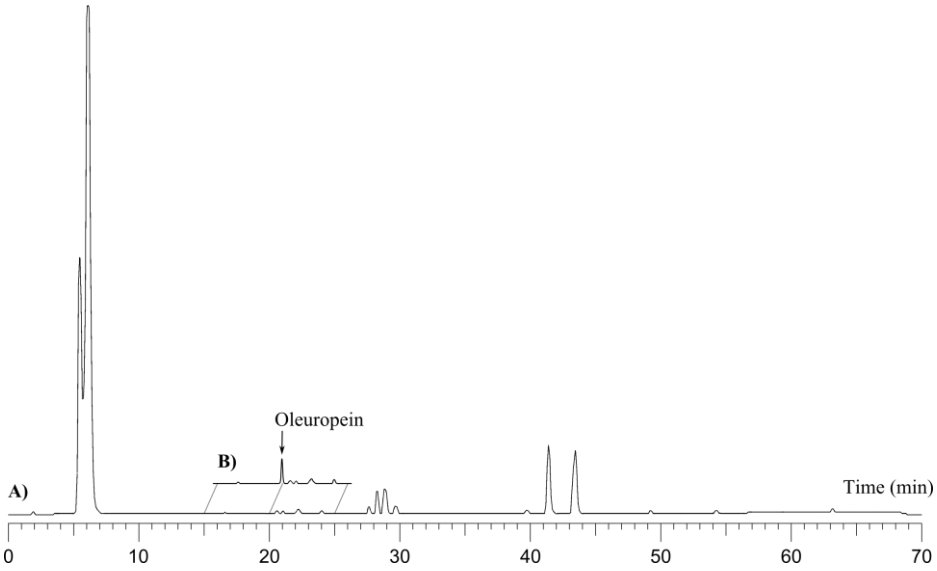

Fig. S22 HPLC chromatogram of the waste stream after being concentrated by the solvent recovery nanofiltration unit (**A**). The waste stream sample was spiked with oleuropein (**B**) to confirm that the waste stream does not contain any product.

11. Green Metrics Calculations

The environmental burden of the continuous process was evaluated through the E-factor and the carbon footprint which are defined in Eq. S21 and Eq. S22, respectively.

$$\text{E-factor} = \frac{\text{kg waste generated}}{\text{kg isolated oleuropein}} \qquad \text{Eq. S21}$$

$$\text{Carbon footprint} = \frac{\text{equivalent kg of } CO_2}{\text{kg isolated oleuropein}} \qquad \text{Eq. S22}$$

Table S7 and S8 break down the continuous process both with and without solvent recovery in terms of energy consumption and waste generation, respectively. The table reveals the individual contribution of each equipment and waste to the total carbon footprint and E-factor of the process. The solid waste of the process was derived from three sources: dissolved matter after the olive leaf digestion (i.e. impurities), the adsorbent and the membrane module. The lifetime of the adsorbent was assumed to be 100 adsorption-regeneration cycles.[11] Each column is filled with 8.11 g of adsorbent, and thus the total amount of adsorbent needed for the production of 1 kg of oleuropein is 0.0676 kg because 417 cycles are required. The dry matter remaining from the olive leaf digestion is not considered as solid waste because they can be used directly as a fertiliser or animal feed.[12] However, the dissolved matter ends up as a concentrated solution at the end of the process and cannot be directly used elsewhere. Consequently, the present study considers incineration to dispose of this waste. The digestion of 1 kg of olive leaves requires 6 L of solvent having 119 g of dissolved matter, out of which 5.8 g is oleuropein. Therefore the total amount of impurities to be disposed of is 20.52 kg per kg of oleuropein. The lifetime, weight and process capacity of an 8″ membrane modules is estimated to be 6 years, 13.5 kg and 22 ML of feed solution, respectively.[13] The isolation of 1 kg of oleuropein requires 2033 L of feed solution which consumes 0.00125 membrane module, eventually generating 20.6 kg of solid waste.

Table S7. Breakdown of energy consumption for the continuous process without and with solvent recovery. The energy consumption is expressed in kilowatts hour per kilogram isolated oleuropein.

	Without solvent recovery		**With solvent recovery**	
	Energy consumption ($kWh.kg^{-1}$)	**Contribution** (%)	**Energy consumption** ($kWh.kg^{-1}$)	**Contribution** (%)
High pressure pump	0.0595	0.0009	1.78	0.028
Recirculation pump	n.a.	n.a.	0.184	0.003
Thermostat (40°C)	2283.3	36.17	2283.3	36.16
Thermostat (25°C)	2024.9	32.08	2024.9	32.07
Thermostat (10°C)	1020.9	16.17	1020.9	16.17
Stirrer (300 rpm)	89	1.41	89	1.41
Olive leaf digestion (40°C)	894.3	14.17	894.3	14.16
Total:	**6312.4**	**100**	**6314.3**	**100**

Table S8. Breakdown of waste generation for the continuous process without and with solvent recovery. The waste generation is expressed in kilogram waste per kilogram isolated oleuropein.

	Without solvent recovery		**With solvent recovery**	
	Waste generation ($kg.kg^{-1}$)	**Contribution** (%)	**Waste generation** ($kg.kg^{-1}$)	**Contribution** (%)
Solvent	1834	98.9	46	69
Adsorbent	0.0676	0.01	0.0676	0.14
Dissolved matter	20.52	1.1	20.52	30.9
Membrane module	n.a.	n.a.	0.00125	0
Total:	**1855**	**100**	**66**	**100**

Both the energy used for the equipment and the waste generated were converted to equivalent CO_2. The low voltage (AC-240 V) electrical energy provided by the UK national grid generates 0.684 equivalents $CO_2 \cdot kWh^{-1}$, while the incineration of chemical and solvent wastes corresponds to 1.98 equivalents $CO_2 \cdot kg^{-1}$.[14] Table R summarizes the carbon footprint of the process expressed in equivalent kg of CO_2 per kg of isolated oleuropein.

Table S9. Breakdown of carbon footprint for the continuous process without and with solvent recovery. The carbon footprint is expressed in equivalent kg of CO_2 per kg of isolated oleuropein.

	Without solvent recovery		**With solvent recovery**	
	Equivalent CO_2 ($kg.kg^{-1}$)	**Contribution** (%)	**Equivalent CO_2** ($kg.kg^{-1}$)	**Contribution** (%)
High pressure pump	0.04	0	1.22	0.03
Recirculation pump	n.a.	n.a.	0.13	0
Thermostat (43°C)	1561.75	19.64	1561.75	35.41
Thermostat (25°C)	1385	17.42	1385	31.4
Thermostat (10°C)	698.3	8.78	698.3	15.8
Stirrer (300 rpm)	60.85	0.78	60.85	1.38
Olive leaf digestion (40°C)	611.72	7.69	611.72	7.69
Solvent	3631.45	45.68	90.8	2.06
Adsorbent	0.04	0	0.04	0
Dissolved matter	1	0.01	1	0.02
Membrane module	n.a.	n.a.	0	0
Total:	**7950**	**100**	**4411**	**100**

References

[1] A. J. Hall, P. Manesiotis, M. Emgenbroich, M. Quaglia, E. De Lorenzi and B. Sellergren, *J. Org. Chem*., 2005, **70**, 1732-1736.

[2] A. R. Katritzky, Y. Zhang and S. K. Singh, *Synthesis*, 2003, **2003**, 2795-2798.

[3] D. Hur, S. F. Ekti and R. Say, *Lett. Org. Chem.*, 2007, **4**, 585-587.

[4] J. Kupai, E. Rojik, P. Huszthy and G. Szekely, *ACS Appl. Mater. Inter.*, 2015, **7**, 9516-9525.

[5] E. Glueckauf, J. I. Coates, J.I., *J. Chem. Soc.*, 1947, **241**, 1315-1321.

[6] S. Sircar, J. R. Hufton, *Adsorption*, 2000, **6**, 137-147

[7] J. R. F. Guedes de Carvalho, J. M. P. Q. Delgado, *Chem. Eng. Sci.*, 2005, **60**, 365-375.

[8] I. B. Valtcheva, P. Marchetti and A. G. Livingston, J. Membrane Sci., 2015, 493, 568-579.

[9] A. De Nino, L. Di Donna, F. Mazzotti, E. Muzzalupo, E. Perri, G. Sindona and A. Tagarelli, Anal. Chem., 2005, 77, 5961-5964.

[10] F. Aouidi, N. Dupuy, J. Artaud, S. Roussos, M. Msallem, I. P. Gaime and M. Hamdi, *Ind. Crop Prod.*, 2012, **37**, 292-297.

[11] J. Kupai, M. Razali, S. Buyuktiryaki, R. Kecili and G. Szekely, *Polym. Chem.*, 2017, **8**, 666-673.

[12] http://www.allaboutfeed.net/Raw-Materials/Articles/2014/2/Olive-leaves-a-good-alternative-to-save-on-feed-costs-1466558W/ (accessed on 24/3/2017)

[13] W. Lawler, Z. Bradford-Hartke, M. J. Cran, M. Duke, G. Leslie, B. P. Ladewig and P. Le-Clech, *Desalination*, 2012, **299**, 103-112.

[14] Carbon Calculations over the Life Cycle of Industrial Activities (CCaLC®), www.ccalc.org.uk